Structural, electronic, and optical properties of NiAl$_3$: First-principles calculations

R. Saniz, Lin-Hui Ye, T. Shishidou,* and A. J. Freeman

Department of Physics and Astronomy, Northwestern University, Evanston, Illinois 60208-3112, USA
(Received 5 November 2004; revised manuscript received 16 March 2006; published 27 July 2006)

We report *ab initio* density-functional calculations of the structural, electronic, and optical properties of NiAl$_3$, using the full-potential linearized augmented plane wave method within the generalized gradient approximation to the exchange-correlation potential. The $D0_{11}$ structure is found to be energetically favorable over both the cubic $L1_2$ and $A15$ phases. The density of states around the Fermi energy, including a pseudogap just above it, is dominated by strongly hybridized Ni d and Al p states. We further present a fully first principles study of the optical properties of NiAl$_3$, using the long wavelength random phase approximation expression for the dielectric function obtained within linear response theory, with full matrix elements. Our calculations cover a large frequency range, extending previous theoretical studies to energies going up to and beyond the effective plasma frequency, which we calculate to be $\sim$16.84 eV. Our results are analyzed in the light of the calculated electronic band structure and density of states, and compared with experimental findings. In the low energy range ($\lesssim$5 eV), where data from different experimental techniques coincide, the calculated reflectivity reproduces very well the main features observed. At higher frequencies, we find a Drude-like behavior, dressed by interband transitions. Our findings invite future measurements that will allow a fuller comparison between theory and experiments.

I. INTRODUCTION

Ordered intermetallics, such as nickel-aluminum alloys, are known to be of great practical interest because of their recurrent applications in advanced materials technology, and for this reason are at the center of many research efforts.[1] In particular, there is an urgent need for an in-depth understanding of the different phases of the Ni-Al phase diagram, as much as for their intrinsic interest as for their relevance to the development of, e.g., possible alternatives to γ-γ' superalloys, and to foster progress in the field of alumalloys in general. As such, the Al-rich phases are of interest, although they have received comparatively less attention than their Ni-rich counterparts. NiAl$_3$ has received increased attention from experimentalists in recent years, however, owing to its potential for several engineering applications.[2] The complicated orthorhombic structure of NiAl$_3$ was completely solved from x-ray powder photographs as early as 1937,[3] and measurements of its magnetic susceptibility[4] and heat of formation[5] were reported by the early 1960s. Among the more recent experimental studies, we mention the x-ray photoelectron spectroscopy (XPS) measurements by Fuggle *et al.*,[6] the ultraviolet photoelectron spectroscopy (UPS) report by Andrews *et al.*,[7] and the spectrophotometric and ellipsometric results of Cubiotti *et al.*[8] On the theoretical side, on the other hand, due to the complexity of the system, discussions have relied for the most part on simplified model calculations. Only rather recently have a few first-principles self-consistent calculations been carried out. We mention the study of the Ni-Al phase diagram by Pasturel *et al.*[9] based on the linear muffin-tin orbital method within the atomic sphere approximation, the reflectivity spectrum at low energy calculated by Mondio *et al.*[10] applying the same method, and the investigation of the thermodynamics of defects in NiAl$_3$ within a pseudopotential approximation.[11] Thus, it is clear that much of the information that can be brought by elec-

tronic structure calculations is still lacking, and that these can contribute importantly to understanding the properties of this material and provide a theoretical framework to discuss the experimental findings mentioned above, among others, while suggesting pathways for future research.

In this work, we carry out first-principles density-functional calculations of the structural, electronic structure and optical properties of NiAl$_3$, using a fully parallelized implementation[12] of the full-potential linearized augmented plane wave (FLAPW) method.[13] From the structural point of view, we find that the experimentally observed $D0_{11}$ structure is energetically favorable over the $A15$ and $L1_2$ structures, the latter being the least favored. NiAl$_3$ is a Hume-Rothery alloy, as already discussed by Trambly de Laissardière and co-workers,[14] exhibiting the pseudogap in the density of states (DOS), typical of these phases, separating bonding and antibonding states. In the $D0_{11}$ structure, the pseudogap falls just above the Fermi level, which is consistent with the XPS and UPS measurements mentioned above.[6,7] The pseudogap is also present in both the $A15$ and $L1_2$ structures. However, in these cases it falls below E_F.

The optical properties of NiAl$_3$ are calculated using the full matrix elements long wavelength expression of the random phase approximation (RPA) result for the dielectric function obtained within linear response theory.[15] The spectrum found, covering energies beyond the effective plasma frequency, calculated to be $\sim$16.84 eV, is essentially accounted for by interband transitions associated with the salient features of the density of states, namely a strong, structured peak of localized Ni d states centered around 2.75 eV below the Fermi energy (E_F), a shoulder just below E_F arising from strongly hybridized Ni d and Al p states, a pseudogap almost 1 eV wide just above E_F, and a region of slowly increasing DOS for energies higher than $\sim$2 eV above E_F, chiefly of Ni pd and Al sp character. Our results for the reflectivity cover essentially the entire spectrum and,

TABLE I. Experimental (room temperature) and calculated ($T=0$ K) lattice constants. The difference of calculated values with respect to experiment is given in parentheses. Lattice constants in Å.

	Experiment[a]	LDA	GGA
a	6.5982	6.5076 (−1.4%)	6.6056 (+0.1%)
b	7.3515	7.2637 (−1.2%)	7.3891 (+0.5%)
c	4.8021	4.7329 (−1.4%)	4.8354 (+0.7%)

[a]Reference 3.

thus, go higher in energy than any previous theoretical study. In the low energy range, where the agreement between the data from different experimental techniques is best established, the structure in the calculated reflectivity corresponds well with the one observed. We further find that for frequencies higher than ~5 eV the reflectivity shows a Drude-like behavior, with a decay softened by interband transitions. Our results are compared with the experimental measurements in Refs. 8 and 10.

This paper is organized as follows: Sec. II is devoted to computational, as well as structural and phase stability considerations. The electronic structure and some of its experimental implications are presented in Sec. III. In Sec. IV, we present our dielectric function and reflectivity results, including a discussion in relation to experiment. A summary and conclusions are presented in Sec. V.

II. STRUCTURAL ASPECTS

NiAl$_3$ crystallizes in the orthorhombic cementite $D0_{11}$ ($oP16$) structure, with space group $Pnma$, and has 16 atoms in the unit cell—4 Ni atoms ($4c$) and 12 Al atoms with two inequivalent positions [Al(1):$4c$, and Al(2):$8d$]—and 14 positional parameters not determined by symmetry.[16] The lattice constants and positional parameters were determined variationally, using 96 **k** points in the irreducible part of the Brillouin zone (IBZ). The muffin-tin radii used for Ni and Al are 3.855 Å and 4.346 Å, respectively (we use the same radius for both types of Al atoms). Also, angular momenta up to $l=8$ were used for both the wave functions and for the charge density representation in the muffin-tin spheres.

In Table I, we give the results obtained for the lattice constants in both the local density[17] (LDA) and generalized gradient[18] (GGA) approximations to the exchange-correlation potential, and make a comparison with experiment. The LDA yields on average lattice parameter values that are slightly below (1.2%–1.4%) the experimental ones

while the GGA gives values that are slightly above (0.1%–0.7%), which is a known trend observed in several other systems.[19] In Table II, we present our results for the positional parameters, again in both LDA and GGA, and compare them with the measurements of Bradley and Taylor.[3] The agreement between our calculated values and experiment is seen to be excellent in both cases. Since the GGA results are slightly closer to experiment overall, our results henceforth are obtained in this approximation.

It is known that some of the transition metal trialuminides possess the cubic $L1_2$ ($cP4$) structure as a metastable phase,[20] which is of interest because this structure offers the possibility of presenting more slip systems than the $D0_{11}$ structure, in which NiAl$_3$ is known to be very brittle. Hence, we compare below the total energy per formula unit for these structures, as well as the heats of formation. We find the total energy difference between the two structures to be $\Delta E = E_{L1_2} - E_{D0_{11}} = 0.773$ eV—which is comparable to the values found between the metastable and stable phases of other transition metal trialuminides.[20]

The heat of formation is calculated to be $\Delta H = -0.41$ eV/atom for the $D0_{11}$ structure, which compares very well with the experimental value of -0.39 eV/atom (5% lower) reported by Hultgren and co-workers.[5,21] On the other hand, the heat of formation corresponding to the $L1_2$ structure is found to be $\Delta H = -0.22$ eV/atom, so that it is 0.19 eV/atom higher than the $D0_{11}$ value. We note that similar results (-0.46 eV/atom for the $D0_{11}$ structure vs -0.26 eV/atom for the $L1_2$ structure) were reported recently by Rasamny and collaborators[11] using a plane wave pseudo-potential method. Now, an alternative crystal structure, not considered before and also potentially having more slip systems, is the $A15$ ($cP8$) structure. In this case, the total energy difference per formula unit with respect to the $D0_{11}$ structure is $\Delta E = E_{A15} - E_{D0_{11}} = 0.739$ eV, i.e., the $A15$ structure is slightly lower in energy than the $L1_2$ structure. The heat of formation for the $A15$ structure is consequently slightly lower as well, namely $\Delta H = -0.23$ eV/atom. Thus, the $D0_{11}$

TABLE II. Experimental (room temperature) and calculated ($T=0$ K) positional parameters.

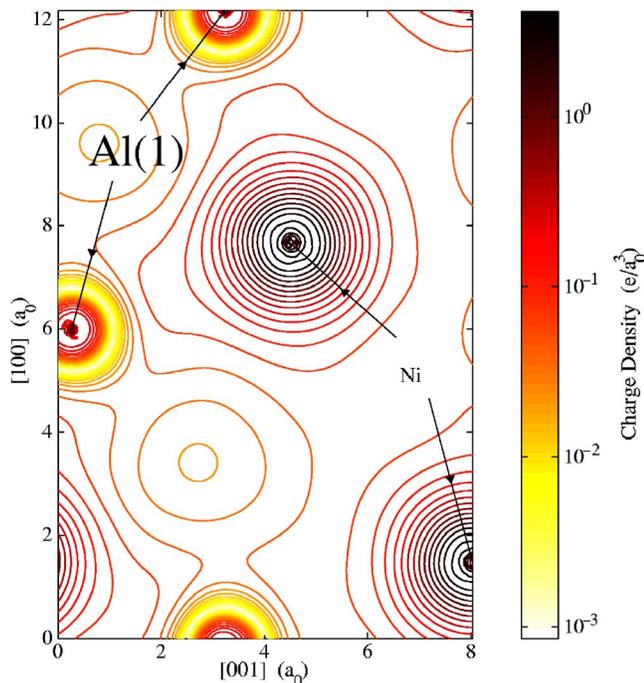|	Experiment[a]			LDA			GGA		
	Ni	Al(1)	Al(2)	Ni	Al(1)	Al(2)	Ni	Al(1)	Al(2)
x	0.869	0.011	0.174	0.872	0.009	0.171	0.872	0.009	0.172
y	1/4	1/4	0.053	1/4	1/4	0.055	1/4	1/4	0.054
z	0.445	0.915	0.356	0.444	0.915	0.361	0.445	0.915	0.360

[a]References 3 and 16.

FIG. 1. (Color online) Electronic charge density on a (010) plane going through $y=1/4$. All five Ni and Al ions shown lie on this plane.

structure is energetically favorable over the $L1_2$ and $A15$ structures by non-negligible amounts.

The calculated bulk modulus (third order Birch-Murnaghan fit) for the $D0_{11}$ structure is $B=113.7$ GPa, while for the $L1_2$ and $A15$ structures we found $B=112.6$ GPa and $B=110.9$ GPa, respectively.[22]

Regarding ductility, it is important to bear in mind that a potential slip vector can be rendered inactive by having a "directional" charge distribution in the direction of the slip vector. This is observed in the case, e.g., of the charge distribution between Ni and Al in the $\langle 111 \rangle$ direction in NiAl.[23] A similar occurrence is observed in $NiAl_3$, as is illustrated here. In Fig. 1, we show the valence charge density contour plot on a (010) plane in the unit cell, with internal coordinate $y=1/4$, containing 2 Ni and 3 Al(1) ions. This directionality may contribute to the brittleness of $NiAl_3$. However, the addition of other transition metals could change the charge distribution and could stabilize some of the higher symmetry phases.[24] In the $A15$ and $L1_2$ structures, given that the pseudogap is below E_F, a lowering of $N(E_F)$ may be achieved by an impurity adding holes and substituting Ni to a percentage sufficient to empty the antibonding states. Thus, transition metal (or other) substitutional addition in $NiAl_3$ represents an important venue for future research.

III. ELECTRONIC STRUCTURE

For the electronic structure results given below, we have used a mesh of 616 **k** points in the irreducible Brillouin zone for increased accuracy. This enables us to make quantitative comparisons with experiment, as shown below. The band
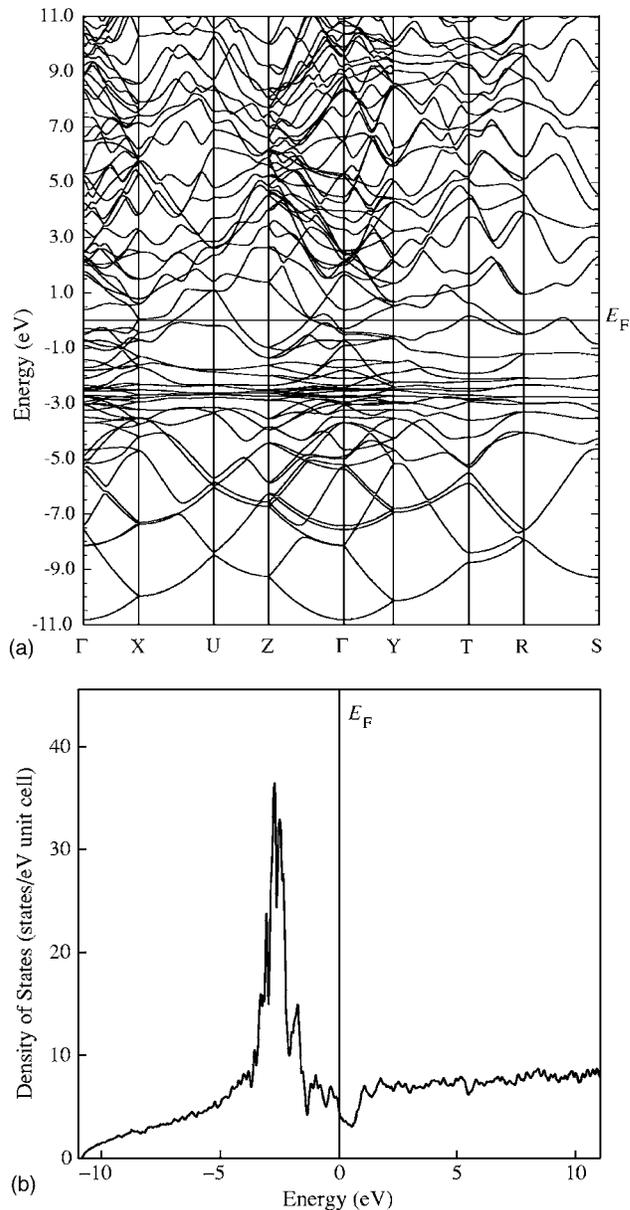

FIG. 2. (a) Electronic band structure calculated within the GGA. Most notable are the strongly localized states centered around -2.75 eV, over an energy range of ~ 2.5 eV. (b) Total density of states, dominated by the strong peak associated with the localized states seen in the band structure ~ 2.75 eV below E_F.

structure of $NiAl_3$ is shown in Fig. 2(a). One notes particularly the strongly localized states between roughly 2 and 4 eV below E_F; these have essentially a Ni $3d$ character. The free-electron character of the states below that energy range arises mainly from Al s and p hybridized states, while the states above have a strong admixture of Ni d and Al p states. The total DOS, shown in Fig. 2(b) is dominated by a strong peak centered at approximately -2.75 eV, in agreement with both XPS (Ref. 6) and UPS (Ref. 7) results; the peak corresponds to the localized Ni states observed in the band structure. Further, as noted in the Introduction, of interest is the pseudogap typical of Hume-Rothery alloys. It falls just above E_F and is ~ 0.8 eV wide. We mention that in the $A15$

and $L1_2$ structures the pseudogap, somewhat narrower, falls 0.5 eV, or more, below E_F. Thus, antibonding states are occupied in these structures, which is reflected in their having a higher ground state energy than the $D0_{11}$ structure.

The muffin-tin sphere-projected *l*-decomposed DOS are shown in Figs. 3(a)–3(c). A comparison of our results with the DOS of pure Ni[25] indicates that the peak in the partial Ni DOS in Fig. 3(a) is essentially due to the collapse of the pure Ni *d* bands into a significantly narrower energy range. A comparison of the pure Al DOS (Ref. 25) with our results in Figs. 3(b) and 3(c) shows that the DOS of the Al 3*s* and 3*p* states is significantly reduced overall. The reduction is stronger for 3*s* states with $-4 \text{ eV} \lesssim E \lesssim 3 \text{ eV}$, indicating a more important charge loss for these states. Thus, the pseudogap in the Al *s* DOS is wider and somewhat deeper than the overall pseudogap. The hybridization of the Ni 3*d* states with the Al 3*p* states at this energy range is clearly stronger than with the Al 3*s* states, and dominates the DOS around E_F, including the (overall) pseudogap. As noted by Trambly de Laissardière *et al.*,[14] and in line with out findings here, the hybridization of the Ni *d* with theAl *sp* states is of great importance for the formation of the pseudogap. Finally, at energies higher than ~ 3 eV, the Al DOS tends to its pure metal behavior. We also note that the calculated DOS reported by Cubiotti *et al.*[26] for $E < 2$ eV, using a so-called extended linear augmented plane wave method, are qualitatively similar to ours.

Regarding the character of the states at E_F, we note that the Ni *d* contribution is much more important than suggested previously, namely approximately 45%, in contrast with the 20%–30% indicated in Ref. 6. This is due to the hybridization mentioned above. Thus, the shoulder observed just below E_F in XPS (Ref. 6) and UPS (Ref. 7) is not only due to Al states, but receives almost as much a contribution from the Ni *d* states. Furthermore, the more recent XPS results of Kovács and collaborators[27] show a shoulder at $E \simeq 1.5$ eV below E_F, interpreted by them as the Ni-*d* Al-*p* shoulder mentioned above, only down shifted in energy. Instead, our results show that it could be due to the peak at $E \simeq -1.75$ eV in the Ni-3*d* DOS, just above the main peak [cf. Fig. 3(a)]. Finally, we note that the total DOS for $E \gtrsim 2$ eV is rather structureless, small oscillations notwithstanding, exhibiting on average a relatively slow increase akin to the quadratic behavior of the DOS for free electronlike metals.[28] This has a bearing on the optical properties we discuss below.

The total DOS at the Fermi energy is $N(E_F) = 4.47$ states/eV unit cell, which, considering experimental results sensitive to $N(E_F)$, leads to further insight into the properties of NiAl$_3$. First, the calculated $N(E_F)$ leads to a Sommerfeld specific heat coefficient of 0.66 mJ/K^2 mol of average atom, which is considerably lower than the experimental value of 1.24 mJ/K^2 mol of average atom reported by Dunlop and collaborators,[29] and indicates a rather important specific-heat mass enhancement ratio $\gamma_{\text{exp}}/\gamma_{\text{band}} = 1.88$. Thus, neglecting many-body effects, the electron-phonon coupling constant is $\lambda_{\text{el-ph}} = 0.88$. This relatively strong value is in line with the results of Dunlop and collaborators[29] on the electrical resistivity of NiAl$_3$, who find a low temperature behavior $\sim T^4$ (down to 4.2 K), indicative of phonon-assisted scattering
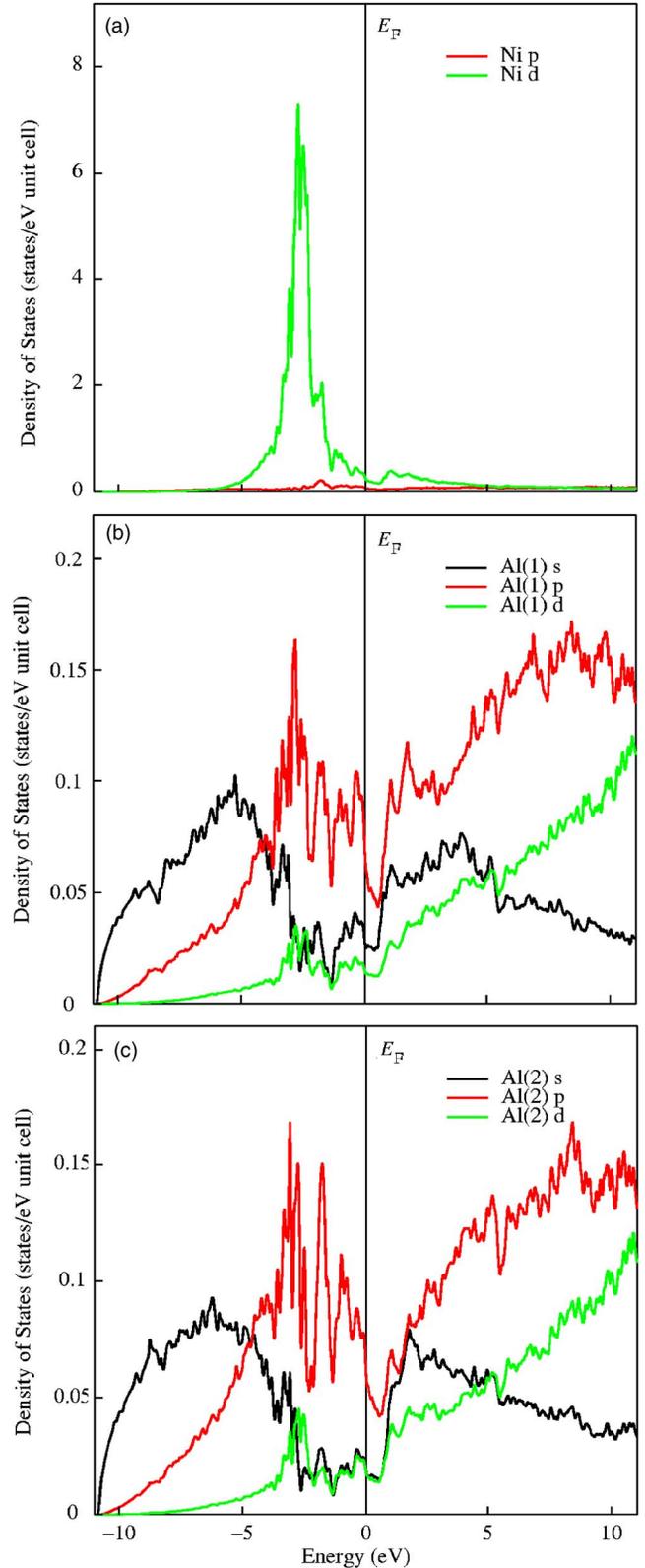

FIG. 3. (Color online) Partial and angular momentum-projected DOS for (a) Ni, (b) Al(1), (c) Al(2). Only the leading projections for each atom type are shown.

contributions to the resistivity. It would be interesting to see measurements of the resistivity and specific heat below

4.2 K to have a closer look at the low temperature properties of $NiAl_3$.

Second, the Pauli paramagnetic susceptibility is calculated to be $\chi_{band} = 2.59 \times 10^{-7}$ emu/g. This $T=0$ K value is to be compared with the experimental magnetic susceptibility, χ_{exp}, reported by Taylor,[4] which ranges from 3.5 $\times 10^{-7}$ emu/g at 77 K to 2.1×10^{-7} emu/g at room temperature. Although the temperature dependence is relatively mild, there is some uncertainty as to the value χ_{exp} will take at $T = 0$ K. However, the experimental values do point to an enhancement ratio $\chi_{exp}/\chi_{band} > 1$. Given that no effectively localized magnetic moments exist in this compound,[4] a result common in dilute alloys of transition metals with free electronlike metals like Al,[30] and that the orbital contributions from localized electrons are quenched by the crystal field, the possible corrections to χ_{band} stem from electron-electron correlations, Landau diamagnetism, and the orbital paramagnetism of itinerant electrons discussed by Kubo and Obata.[31] The enhancement ratio found above appears to indicate that Landau diamagnetism is overcome by the other two effects. Electron spin resonance and gyromagnetic ratio measurements would be particularly welcome to advance further in this direction.

IV. OPTICAL PROPERTIES

We now turn to the optical properties studied by Cubiotti and co-workers[8] and by Mondio and co-workers.[10] The imaginary part of the dielectric function can be obtained in the framework of linear response theory, within the random phase approximation. In the long wavelength limit we have[15]

$$\epsilon_2(\omega) = \frac{8\pi^2 e^2}{\omega^2 m^2 V} \sum_{i \in c, f \in v} \sum_{\mathbf{k}} |\langle \mathbf{k}, i | \hat{\mathbf{e}} \cdot \mathbf{p} | \mathbf{k}, f \rangle|^2$$
$$\times \delta[E_i(\mathbf{k}) - E_f(\mathbf{k}) - \hbar\omega], \quad (1)$$

where V is the unit cell volume and the sum over i (f) is restricted to conduction (valence) band states. We calculate $\epsilon_2(\omega)$ over a large range of frequencies (up to ~ 30 eV) using a fine mesh of 4794 $\mathbf{k}$ points in the IBZ, and up to 176 states.[32] In metallic systems it is important to include the Drude contribution to the dielectric function $1 - \omega_p^2/(\omega^2 + i\omega\gamma)$. The Drude plasma frequency is calculated in terms of the momentum matrix elements and the $\omega \to 0$ limit in Eq. (1). For the three different polarizations we find $\omega_{pxx} = 4.43$ eV, $\omega_{pyy} = 5.31$ eV, and $\omega_{pzz} = 4.63$ eV, whence $\omega_p^2 = (\omega_{pxx}^2 + \omega_{pyy}^2 + \omega_{pzz}^2)/3 = 4.81$ eV. Our results are markedly different from those in Ref. 8, particularly for ω_{pzz}. We do not know the reason for the discrepancy, but we note that the mesh used by those authors is much coarser (196 $\mathbf{k}$ points), leading to a larger uncertainty in some of their calculated values. For the damping factor we take a value $\gamma = 0.025$ eV, corresponding to room temperature. The real part, $\epsilon_1(\omega)$, is obtained by means of the Kramers-Kronig relation. Further, the effective plasma frequency is calculated through the sum rule $\omega_p'^2 = (2/\pi) \int_0^\infty d\omega \omega \epsilon_2(\omega)$, yielding a value $\omega_p' = 16.88$ eV. Thus, interband excitations are largely responsible for the effective plasma frequency value.
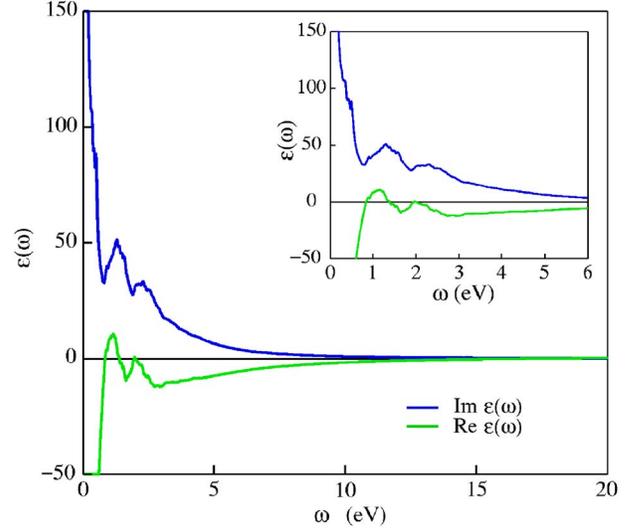

FIG. 4. (Color online) Real and imaginary parts of the dielectric function $\epsilon(\omega)$ exhibiting the structure associated with interband transitions, as discussed in the text. Inset: Enlargement over the 0–6 eV range.

We show $\epsilon_1(\omega)$ and $\epsilon_2(\omega)$ in Fig. 4, for frequencies up to 20 eV. The inset shows an enlargement over the low frequency range (0–6 eV). The structure in $\epsilon_2(\omega)$ at low ω is understood as follows. The shoulder at 0.5 eV is due to transitions from the peak just below E_F in the DOS to the Fermi level. The broad maximum centered at ~ 1.25 eV is mainly due to transitions from the peak just below E_F in the DOS to the states in the region of increased DOS starting at ~ 1 eV above E_F. The second maximum, centered at ~ 2.3 eV and also broad, is essentially due to transitions from the upper edge of the d-band manifold to E_F. Moreover, $\epsilon_1(\omega)$ shows the effective plasma frequency, ω_p', to occur at ~ 16.84 eV, which is in excellent agreement with the value obtained above through the sum rule. For frequencies above ~ 5 eV, both $\epsilon_1(\omega)$ and $\epsilon_2(\omega)$ show a Drude-like behavior.

A direct comparison with experiment is provided by the calculated reflectivity $R(\omega)$, which we show in Fig. 5(a) (again, the inset shows an enlargement over the low frequency range). We show in Fig. 5(b) the spectrophotometric [curve (a)] and the REELS [curve (b)] results from Ref. 10. Note that our calculation covers energies going up to 30 eV, representing nearly the entire reflectivity spectrum. Besides the structure for $\omega \lesssim 5$ eV, which we discuss below, $R(\omega)$ varies in a way typical of metals for frequencies approaching ω_p', decaying gradually as $\epsilon_2(\omega)$ tends to zero and the material becomes transparent. The decay, however, is softened and broadened by interband transitions. In the low energy range our results generally agree with the experimental results in Refs. 8 and 10, although a definite comparison is rendered difficult by the fact that the data reported, covering different energy ranges, present some uncertainty and differ to a certain extent. The spectrophotometric data,[8] the ellipsometric data,[8] and the REELS data[10] all show a rapid initial fall from above 0.9 to a minimum located at $\omega \simeq 1$ eV, followed by a maximum at 1.5 eV, in coincidence with our results in Fig. 4. The ellipsometric and the REELS data show
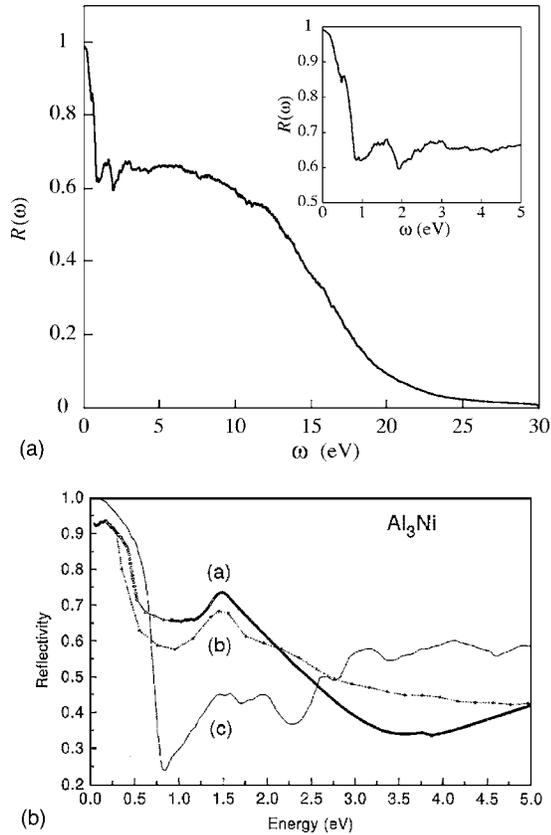
FIG. 5. (a) Calculated reflectivity spectrum; the inset shows an enlargement of the 0–5 eV range. (b) Spectrophotometric [curve (a)] and REELS [curve (b)] results reported by Mondio *et al.* (Ref. 10) [curve (c) is a LTMO-ASA calculated result]; reproduced with permission.

a further shoulder between 2 and 2.5 eV, while our results show a maximum at ~2.8 eV, which may be associated with this shoulder. The spectrophotometric data, on the other hand, show no shoulder in this energy range, but a monotonic decrease reaching a minimum at ~3.5 eV. However, Mondio and co-workers indicate[10] that some unresolved structure in the spectrophotometric data could be present at these energies. The ellipsometric data do not go beyond ω > 3.5 eV. The spectrophotometric data, covering frequencies up to 6 eV, show another broad maximum at around 5.5 eV, while it is absent in the REELS data; our results do not show any clear structure at this frequency and our DOS and dielectric function do not seem to suggest any particular feature there.

The REELS results are the only ones covering the spectrum to higher frequencies—up to 35 eV. For energies above 5 eV, there is a clear difference between our results for $R(\omega)$ and those calculated[10] from the REELS measurements. While the REELS result shows a very broad maximum centered roughly at 14 eV, in our result $R(\omega)$ is already decaying in that energy range, as stated above. The decay in the REELS data is pushed to higher frequencies by 5 eV, or more, and appears to be less steep. We do not see a clear reason for the discrepancy. Part of it could be that in this energy range self-energy corrections outside the scope of our

treatment start to have a more important effect on the energy spectrum. On the other hand, as stressed by Mondio and collaborators,[10] REELS is essentially a surface technique, so that the bulk properties may be incompletely represented and/or masked by surface effects. A measurement of the plasma frequency, e.g., in an EELS experiment, would provide an important reference point to characterize and understand the optical properties of NiAl$_3$. Thus, it would be desirable to see further experimental measurements, with the above or other techniques, covering a wider energy range.

V. SUMMARY

In summary, we presented first principles calculations of the structural, electronic, and optical properties of NiAl$_3$. We find that the experimentally observed $D0_{11}$ structure is energetically favorable over the $L1_2$ and $A15$ structures. The band structure presents a manifold of states with little dispersion, centered at ~2.75 eV below E_F, arising from Ni d states and generating a dominant peak in the density of states. The density of states also shows a pseudogap just above the Fermi level. The $L1_2$ and $A15$ structures also exhibit the pseudogap, but below the Fermi level, so that the filling of antibonding states appears to raise their ground state energy above that of the $D0_{11}$ structure. While our results generally agree with experiment, we predict some additional structure which we hope current resolution will be able to resolve. Also, the density of states around the Fermi energy, including the pseudogap region, is dominated by strongly hybridized Ni d and Al p states.

We also presented a fully first principles study of the optical properties of NiAl$_3$, using the long wavelength RPA expression for the dielectric function obtained within linear response theory. Our calculation extends previous theoretical studies to frequencies up to 20–30 eV. The main features observed in the low energy range (below 5 eV), where the different data reported coincide, are well reproduced by our results. At higher frequencies, we find both the dielectric function and the reflectivity to be Drude-like—dressed by interband transitions, with an effective plasma frequency calculated to be ~16.84 eV. At these higher frequencies, however, the agreement between our calculated reflectivity and experiment is poor, as the REELS data show a very broad maximum centered roughly around 14 eV while in our results the reflectivity is already decaying at that energy range. The decay in the REELS measurements also appears to be less steep and starts at higher frequency. We look forward to future measurements that will allow a fuller comparison between theory and experiment.

*Present address: Department of Quantum Matter, ADSM, Hiroshima University, Higashihiroshima 739-8530, Japan.

[1] For reviews see, e.g., *Ordered Intermetallics—Physical Metallurgy and Mechanical Behaviour*, Vol. 213 of NATO Advanced Science Institutes, Series E: Applied Sciences, edited by C. T. Liu, R. W. Cahn, and G. Sauthoff (Kluwer Academic, Dordrecht, 1992); J. E. Payne and P. D. Desai, *Properties of Intermetallic Alloys I. Aluminides* (Center for Information and Numerical Data Analysis and Synthesis, Purdue University, West Lafayette, IN, 1994); in *Intermetallics for the Third Millenium*, edited by S. C. Deevi, C. T. Liu, and M. Yamaguchi, Intermetallics **8**, Nos. 9–11 (2000).

[2] K. Yamashita, I. Fujimoto, T. Kurakumo, S. Kumai, and A. Sato, Philos. Mag. A **80**, 219 (2000); T. Marcelo, M. H. Carvalho, E. B. Lopes, J. D. Bartout, and Y. Bienvenu, Key Eng. Mater. **230**, 189 (2002); P. Barutška, J. Lašek, and V. Paidar, Surf. Eng. **19**, 185 (2003); P. Yu, C. J. Deng, N. G. Ma, and D. H. L. Ng, J. Mater. Res. **19**, 1187 (2004).

[3] A. J. Bradley and A. Taylor, Philos. Mag. **23**, 1049 (1937).

[4] M. A. Taylor, Proc. Phys. Soc. London **78**, 1244 (1961).

[5] R. Hultgren, R. L. Orr, P. D. Andersen, and K. K. Kelley, *Selected Values of Thermodynamic Properties of Metals and Alloys* (Wiley, New York, 1963).

[6] J. C. Fuggle, F. U. Hillebrecht, R. Zeller, Z. Zolnierek, P. A. Bennett, and C. Freiburg, Phys. Rev. B **27**, 2145 (1982).

[7] P. T. Andrews, S. C. Millar, G. Cubiotti, Yu. N. Kucherenko, A. N. Yaresko, and V. N. Antonov, J. Phys.: Condens. Matter **5**, 1935 (1993).

[8] G. Cubiotti, A. D. Laine, G. Mondio, E. E. Krasovskii, O. V. Krasovska, Yu. N. Kucherenko, V. N. Antonov, Yu. V. Kudryatsev, and V. G. Ivanchenko, J. Phys.: Condens. Matter **8**, 2549 (1996).

[9] A. Pasturel, C. Colinet, A. T. Paxton, and M. van Schilfgaarde, J. Phys.: Condens. Matter **4**, 945 (1992).

[10] G. Mondio, A. D. Laine, A. M. Mezzasalma, G. Cubiotti, and Yu. N. Kucherenko, J. Electron Spectrosc. Relat. Phenom. **85**, 1 (1997).

[11] M. Rasamny, M. Weinert, G. W. Fernando, and R. E. Watson, Phys. Rev. B **64**, 144107 (2001).

[12] T. Shishidou, L.-H. Ye, M. Weinert, and A. J. Freeman (unpublished).

[13] E. Wimmer, H. Krakauer, M. Weinert, and A. J. Freeman, Phys. Rev. B **24**, 864 (1981); M. Weinert, E. Wimmer, and A. J. Freeman, *ibid.* **26**, 4571 (1982); H. J. F. Jansen and A. J. Freeman, *ibid.* **30**, 561 (1984).

[14] G. Trambly de Laissardière, D. N. Manh, L. Magaud, J. P. Julien, F. Cyrot-Lackmann, and D. Mayou, Phys. Rev. B **52**, 7920 (1995).

[15] See, e.g., P. O. Nilsson, in *Solid State Physics*, Vol. 29, edited by H. Ehrenreich, F. Seitz, and D. Turnbull (Academic, New York, 1974), p. 139.

[16] *Pearson's Handbook of Crystallographic Data for Intermetallic Phases*, edited by P. Villars and L. D. Calvert (American Society of Metals, Metals Park, OH, 1985).

[17] L. Hedin and B. I. Lundqvist, J. Phys. C **4**, 2064 (1971).

[18] J. P. Perdew, K. Burke, and M. Ernzerhof, Phys. Rev. Lett. **77**, 3865 (1996).

[19] See, e.g., C. Stampfl, W. Mannstadt, R. Asahi, and A. J. Freeman, Phys. Rev. B **63**, 155106 (2001).

[20] See, e.g., J. H. Xu and A. J. Freeman, Phys. Rev. B **40**, 11927 (1989); **41**, 12553 (1990).

[21] In the heat of formation calculations, Ni was taken in the ferromagnetic state. The calculated magnetic moment is $0.621\mu_B$ per unit cell, which is close to the experimental value of $0.616\mu_B$ [see H. Danan, A. Herr, and J. P. Meyer, J. Appl. Phys. **39**, 669 (1968)].

[22] We were unable to find reports on the experimental bulk modulus of $NiAl_3$; the only calculated value we found is that of Trambly de Laissardière *et al.*, who calculated a value $B=132$ GPa. See Ref. 14.

[23] A. J. Freeman, J. Xu, T. Hong, and W. Lin, in *Ordered Intermetallics—Physical Metallurgy and Mechanical Behaviour*, Vol. 213 of NATO Advanced Science Institutes, Series E: Applied Sciences, edited by C. T. Liu, R. W. Cahn, and G. Sauthoff (Kluwer Academic, Dordrecht, 1992).

[24] For instance, it has been shown that $ZrAl_3$ can be stabilized in its cubic phase by the addition of Sc. See Ref. 20.

[25] D. Papaconstantopoulos, *Handbook of the Band Structure of Elemental Solids* (Kluwer Academic, New York, 1986).

[26] G. Cubiotti, E. E. Krasovskii, O. V. Slobodyan, Yu. N. Kucherenko, and V. N. Antonov, J. Phys.: Condens. Matter **7**, 4865 (1995).

[27] Zs. Kovács, L. Kövér, P. Weightman, D. Varga, R. Sanjinés, J. Pálinkás, G. Margaritondo, and H. Adachi, Phys. Rev. B **54**, 8501 (1996).

[28] The increase is slow on the scale of the very high DOS below E_F arising from the Ni d states.

[29] J. B. Dunlop, G. Grüner, and A. D. Caplin, J. Phys. F: Met. Phys. **4**, 2203 (1974).

[30] N. W. Ashcroft and N. D. Mermin, *Solid State Physics* (Saunders College, Philadelphia, 1976), p. 685.

[31] R. Kubo and Y. Obata, J. Phys. Soc. Jpn. **11**, 547 (1956).

[32] The $D0_{11}$ structure being of orthorhombic symmetry, its optical properties depend on the polarization of the incident light. The calculated dielectric function and reflectivity discussed in this work are averaged over the three orthogonal polarizations.